JOURNAL OF CATALYSIS 83, 61–78 (1983)

In Situ Transmission Electron Microscope Studies of Palladium on MgO

K. HEINEMANN, T. OSAKA,[1] H. POPPA, AND M. AVALOS-BORJA

Stanford/NASA Joint Institute for Surface and Microstructure Research, Department of Materials Science and Engineering, Stanford University, Stanford, California 94305

Received September 23, 1982; revised April 19, 1983

Palladium particles were grown from the vapor phase inside a controlled-vacuum specimen chamber of a transmission electron microscope (TEM) on freshly prepared and flat MgO substrate surfaces. Annealing and various effects of gas exposure of the particulate Pd deposits were studied *in situ* by high-resolution TEM and electron diffraction. Even at substrate temperatures of 300°K (room temperature), the deposits were perfectly epitaxial. A lattice expansion of 2–4% was noted; the highest values of expansion (compared to the bulk Pd lattice parameter) were found for the smallest particles (1–1.5 nm size range). Long-time RT exposure of Pd/MgO in a vacuum of 10^{-8} mbar (major residual gas components were water and nitrogen) yielded negligible particle mobility and coalescence. However, exposure to laboratory air or oxygen at RT greatly enhanced the particle mobility and coalescence and also resulted in flattening of the deposit particles. Electron-beam irradiation further enhanced this effect. Exposure to laboratory air for several tens of hours led to strong coalescence with a tendency of minimization of the particle surface areas by promoting three-dimensional Pd particle habit formation. The results, therefore, indicate that small deposited metal particles may undergo appreciable changes when they are exposed to air at RT, such as is common practice in *ex situ* TEM investigations of particulate deposits.

INTRODUCTION

Advanced model catalytic studies have spurred a renewed interest in small-particle research, and the transmission electron microscope (TEM) has become the key instrument for the determination of the crystal structure and habits of nanometer-size particles (*1, 2*). In the vast majority of all such work reported, the particles were prepared (i) outside the vacuum system in which they were subsequently investigated, and (ii) often many hours or days before inspection by TEM actually started, and little if any attention has been directed to the influence that this pretreatment of the metal deposit might have had on the TEM results. In the present work we have employed *in situ* TEM, where the depositions and subsequent TEM analysis are performed in the same vacuum vessel under controlled vacuum conditions (*1*), for the study of this effect.

As important as controlled vacuum conditions—achieved in our *in situ* approach by replacing the regular TEM specimen chamber with a uhv-compatible advanced custom chamber that is differentially pumped—is the availability of clean substrates for such work. Single crystal thin, electron transparent films of MgO (*3, 4*) can be produced by *in situ* electron-beam flash heating of chemically prethinned MgO disks. Since a reasonable "cleanliness" of this type of substrate has been well documented, and since MgO is a substrate of interest in catalysis, sometimes exhibiting strong metal/substrate interaction, we have chosen MgO as substrate for this work.

Since our *in situ* TEM facility also operates under high image resolution conditions, we were able to study not only epitaxy and pseudomorphism, but also the nucleation and early growth of the Pd particles from the vapor phase, and their exposure to various gases at room temperature.

[1] On leave from Waseda University, Tokyo, Japan.

0021-9517/83 $3.00

EXPERIMENTAL

Palladium was evaporated from an electron-beam heated source installed in a custom stainless-steel specimen chamber fitted to a Siemens Elmiskop 101 transmission electron microscope (TEM) converted for *in situ* experimentation (*5*). The evaporation rate and deposit thickness were monitored with a quartz crystal microbalance. A rate of 3×10^{13} atoms/cm^2/s was maintained for all depositions. The maximum mean deposit thickness was 1.8 nm, if unity sticking probability on the quartz crystal is assumed. The chamber, evacuated with a helium cryopump, was at a base pressure in the mid 10^{-9} mbar range (1 mbar = 0.75 Torr) before and after the depositions. Because of the particular evaporation source used, the pressure increased by approximately 1 order of magnitude during the depositions.

In order to minimize the influence of the imaging electron beam, its intensity was maintained below 0.1 A/cm^2, and the total beam exposure of the specimen areas of interest was minimized to below a few tens of A s/cm^2 (1.0 A s/cm^2 = 6242 electrons/nm^2) by performing all routine TEM image adjustments at specimen regions outside those of interest, except for experiments where specimen irradiation damage itself was the object of the investigation.

Magnesium oxide substrates were prepared from 0.5-mm-thick MgO disks of 3 mm diameter by chemical prethinning with hot, concentrated phosphoric acid in a dual-jet TEM specimen thinning apparatus until a hole formed in the center of the disk. The prethinned specimen was then washed carefully in methanol and inserted in the hot stage of the TEM. Clean, electron-transparent areas of MgO in {100} and {111} orientation were obtained by electron-beam flash heating immediately prior to beginning the deposition (*3*): a selected specimen area (near the edge of the hole) was exposed to a beam of approximately 15 μm in diameter at 2–8 A/cm^2 intensity for a fraction of a second, regulated by passing with the final condenser lens through focus (*4, 6, 7*). This preparation of clean, electron-transparent specimen areas by flash heating could be repeated several times in other sample regions for additional deposition experiments. The high momentary temperature conditions associated with this technique cause any deposits, including previous palladium islands and hydrocarbon contaminants, should they be present, to evaporate (*5*), thus leaving clean substrate surfaces regardless of the deposition history of the sample. Most depositions were performed at room temperature.

A typical experimental sequence consisted of (a) preparation of a clean, single crystal specimen area, (b) evaporation of palladium (usually with the imaging electron beam off), and (c) the generation of a defocus series of high resolution TEM images and of a few selected-area diffraction (SAD) patterns. Step (c) was sometimes repeated after various time intervals of high-vacuum, RT-"annealing," or after admitting gases (oxygen or hydrogen at low pressures, typically for several hundred Langmuirs, or laboratory air at atmospheric pressure). In a few cases, the sample was transferred to a high-resolution Hitachi H-500H TEM for extended-period air exposure and selected-zone dark field (SZDF) work (*8*).

The resulting electron micrographs were evaluated in terms of palladium island number density, surface coverage, and particle size distribution using a Zeiss Videomat image analyzer.

RESULTS

Early Growth and Vacuum Anneal

As known from our previous work, the MgO substrate preparation method by electron-beam flash heating produces two types of substrate orientations, {100} and {111}. Since {100} surfaces were produced much more frequently, and since there were no indications that the major results were de-

pendent on the orientation of the substrate surface, we are reporting here mostly results obtained on {100} MgO.

A sequence of images of typical room temperature (RT) deposits of 0.3, 0.6, 1.2, and 1.8 nm nominal thickness on {100} MgO is shown in Fig. 1. The number density of the palladium islands, the area coverage, and the average particle size are plotted in Figs. 2–4. Whereas the determination of area coverages with an image analyzer working on the principle of gray level discrimination is quite reliable, the measurement of mean particle sizes or size distributions can be quite ambiguous for small particles, since the gray-level contrast of such particles depends strongly on the TEM focus condition and on background intensity variations. We have, therefore, relied on a calculation rather than a measurement of the mean particle diameter (D_m). If Θ is the measured area coverage ($0 < \Theta < 1$), if N is the measured particle number per cm^2, and if we assume circular particle projections and hemispherical particle shapes, we get

$$\Theta \approx 10^{-14} N\pi \frac{D^2}{4} \qquad (1)$$

and therefore

$$D \approx 1.1 \times 10^7 (\Theta/N)^{1/2} \qquad (2)$$

A typical deposition–annealing sequence (all at RT) is presented in Fig. 5, showing in (a) the as-"cleaved" MgO substrate, in (b) the 0.3-nm Pd deposit shortly after deposition, and in (c) the same deposit after 21 h annealing at background pressure. Careful examination of the figure indicates that some coalescence events and mobility events (one example each is shown in the circle and the square, respectively) occurred under these RT, high vacuum (2×10^{-8} mbar) annealing conditions. The effect of high vacuum, low-temperature annealing decreases with increased average deposit thickness. For twice the deposit thickness, much fewer coalescence events were found, and practically no annealing effect was noted for deposits of more than 1.2 nm average thickness.

Epitaxy and Lattice Expansion

In Fig. 6 we present two typical diffraction patterns representative of 1.2- and 1.8-nm deposits of Pd on {100} MgO. Apart from the fact that the patterns reveal near to perfect epitaxy for these RT deposits (which can also be considered a good check on the substrate cleanliness), one can notice that the Pd diffraction spots are relatively broad, and measurements of the spot spacings, using the perfect MgO 200- and 220-type spots as internal standard, indicate that the corresponding lattice parameter is substantially larger than that of bulk palladium. Measurements using results from several diffraction patterns and from several depositions for each thickness indicate that this "lattice expansion" amounts to 2.5–3% for deposits thicker than 0.9 nm (average), and that it increases notably for thinner deposits. No changes in the diffraction patterns were observed upon RT annealing or exposure of the deposits to gases or laboratory air. It should be noted, however, that our experiments do not allow any conclusion whether the entire unit cell is expanded, or if the expansion observed in the direction parallel to the substrate surface is concomitant with less expansion or even contraction in the direction normal to the substrate surface, thus reducing the unit cell volume increase. Information about lattice expansion on {111} MgO was not obtained because of difficulties in the measurement of MgO d-spacings which are subject to changes due to strong bending and concomitant diffraction contrast changes within even small selected areas.

Gas Exposures

Exposure of Pd/MgO deposits to oxygen or air at RT yielded marked changes beyond those that are obtained during RT vacuum annealing alone. An example for a 0.3-nm deposit is presented in Fig. 7, showing the conditions 7 min after deposition in

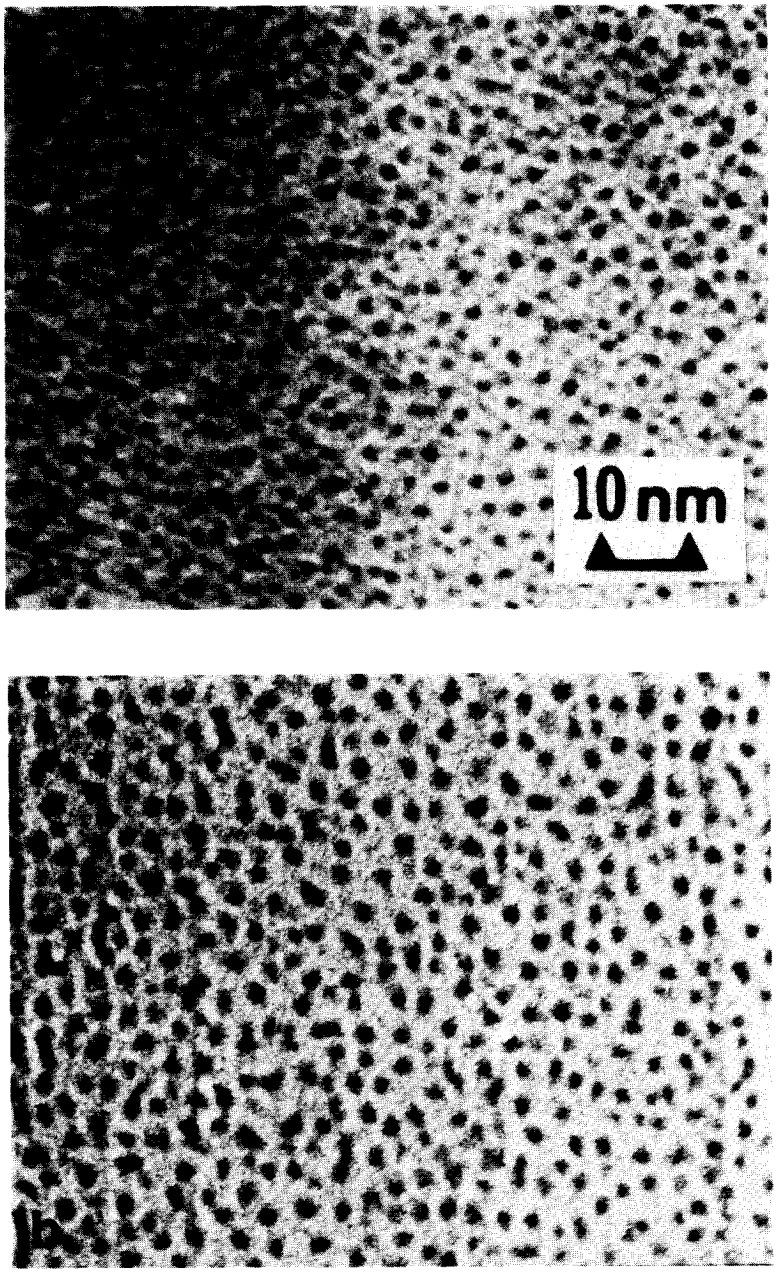

FIG. 1. Typical room temperature (RT)-deposit of Pd on {100} MgO; nominal thickness 0.3 nm (a), 0.6 nm (b), 1.2 nm (c), and 1.8 nm (d).

(a) and 2.5 min following subsequent oxygen exposure at 2×10^{-6} mbar for 3 min in (b). The circles in (b) indicate some of the many coalescence events that have occurred due to the oxygen exposure. The triangle denotes a particle that has changed into a distinct, triangular shape. Further mobility during a few hours of additional annealing was then relatively infrequent. This result indicates that due to the oxygen exposure (initiated 12 min after the end of the deposition) we observe particle mobility

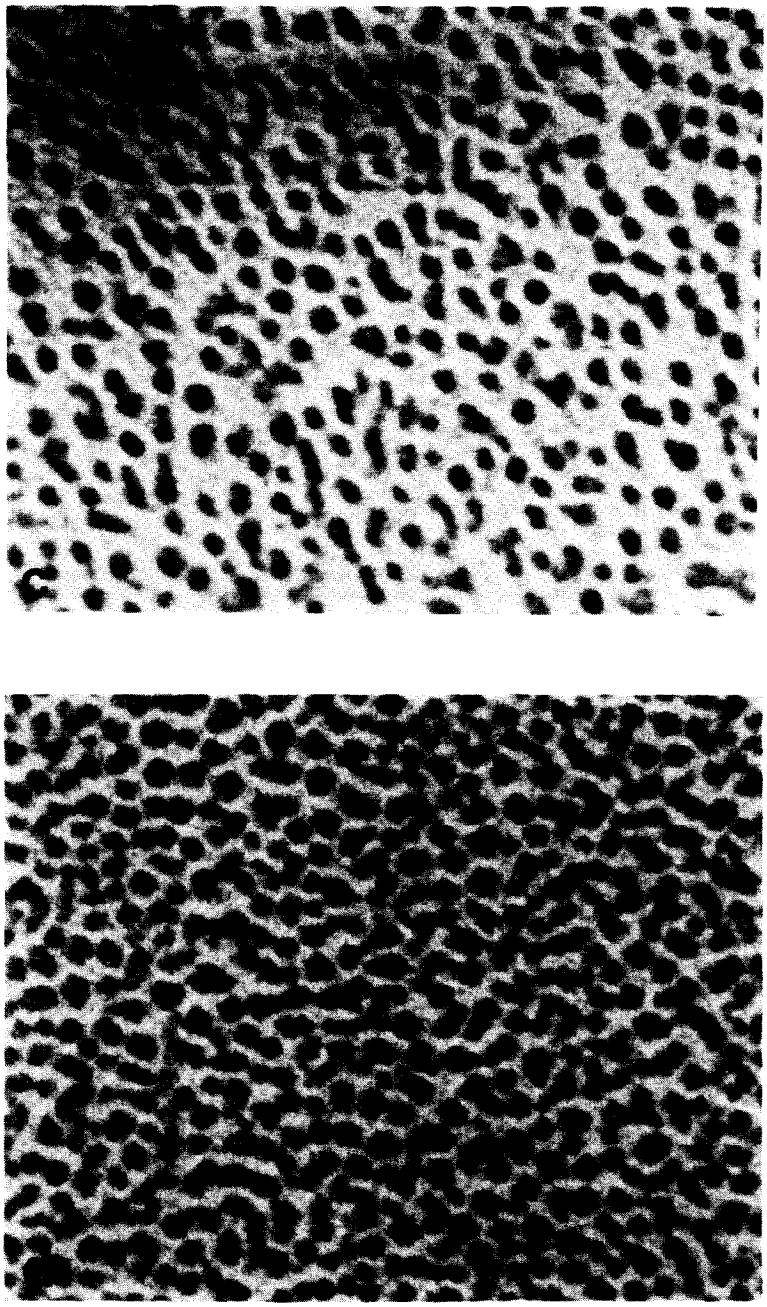

FIG. 1—*Continued.*

and coalescence as in the case vacuum annealing, but that the relative number of events is markedly increased.

More significant changes are observed if thin Pd/MgO deposits are exposed for short durations to laboratory air at atmospheric pressure. Even in the case of a relatively thick deposit (0.9 nm), where vacuum annealing yields virtually no changes, the particle number density was observed to decrease by as much as 16%, and the decoration of substrate surface steps be-

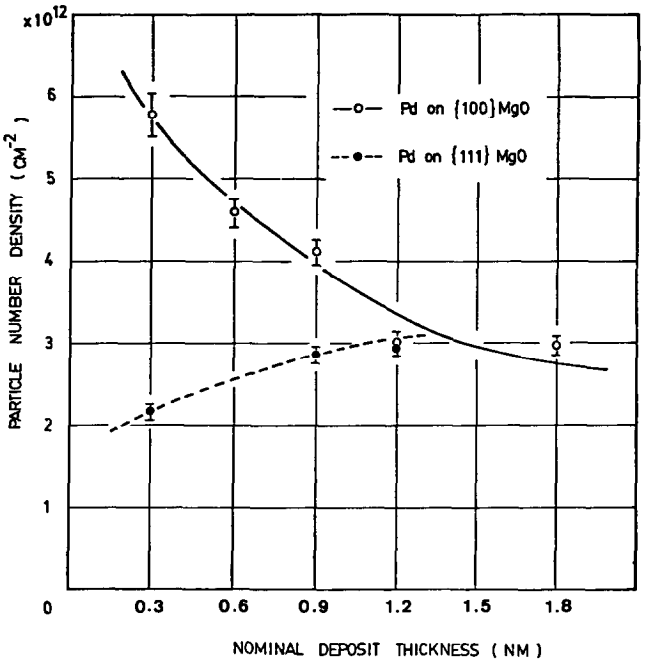

FIG. 2. Particle number density vs nominal deposit thickness for Pd grown on MgO {100} and {111} at RT.

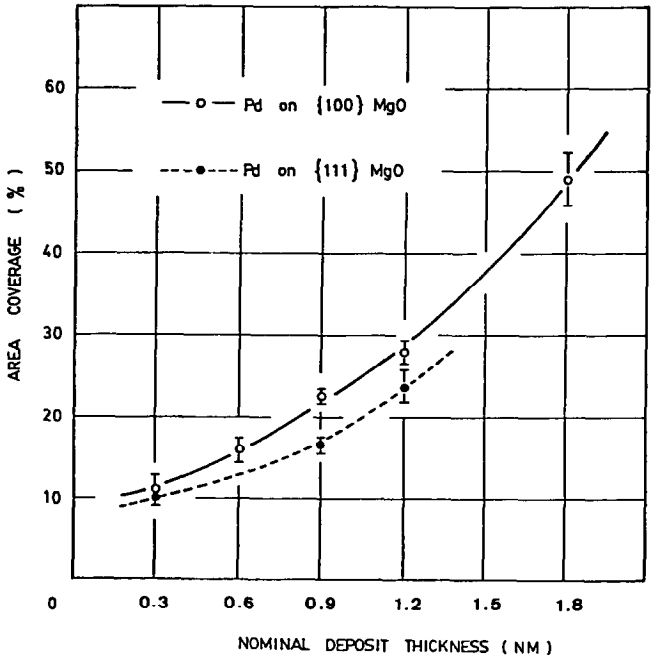

FIG. 3. Particle area coverage vs nominal deposit thickness for Pd grown on MgO {100} and {111} at RT.

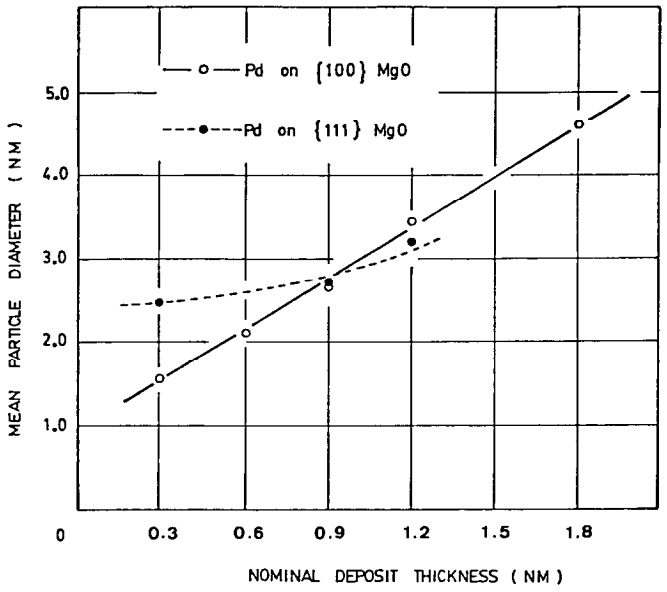

FIG. 4. Mean particle diameter, computed from Eq. (2), vs nominal deposit thickness for Pd grown on MgO {100} and {111} at RT.

came more pronounced. In Fig. 8 we present an example of a yet thicker RT deposit (1.8 nm) that had been exposed to air three times, once for 10 min while still in the specimen stage of the *in situ* TEM facility (Fig. 8b), once for some 30 min during subsequent transfer to the Hitachi H500H high-resolution microscope (Fig. 8c), and once for 120 h in a long-term laboratory air exposure experiment (Fig. 8d). One can see that the particles have moved toward each other, often forming chains of particles that have coalesced but not yet sintered into new, homogeneous single crystal, hemispherical particles. The changes are most pronounced between the as-deposited stage (Fig. 8a) and the first air exposure (Fig. 8b), and the process continued during the second air exposure at a slower rate. However, the changes due to exposure to laboratory air apparently continue to occur for long times. Figure 8d reveals a substantial additional change after 120 h of air exposure. Whereas the previous particle shapes had predominantly been square or rectangular, most facets seemed to have disappeared during the prolonged air exposure, leaving chains of particles with essentially round profiles. But even in this progressed stage of coalescence—there is also a significant number of additional coalescence events in Fig. 8d when compared to Fig. 8c—complete sintering into new, homogeneous single crystal particles has not occurred. This was demonstrated with selected-zone dark-field (SZDF) microscopy (*8*), where images produced with the Pd 200 zone clearly indicate separate Pd diffraction intensities, still stemming from the original, then separated crystallites (Fig. 9). The SZDF work also indicated that the ⟨001⟩ direction in the deposit is at an unexpected 45-degree angle with respect to substrate surface steps.

The long-term annealing effect was quite different if the annealing, following a few minutes of exposure to laboratory air at atmospheric pressure, was performed *in vacuo* (1×10^{-8} mbar). The result was then the same as for long term annealing of oxygen-exposed samples. An example is shown in Fig. 10 for the case of a 0.3-nm Pd deposit on MgO 40 min after (left) and 100 h after such treatment (3 min exposure to ox-

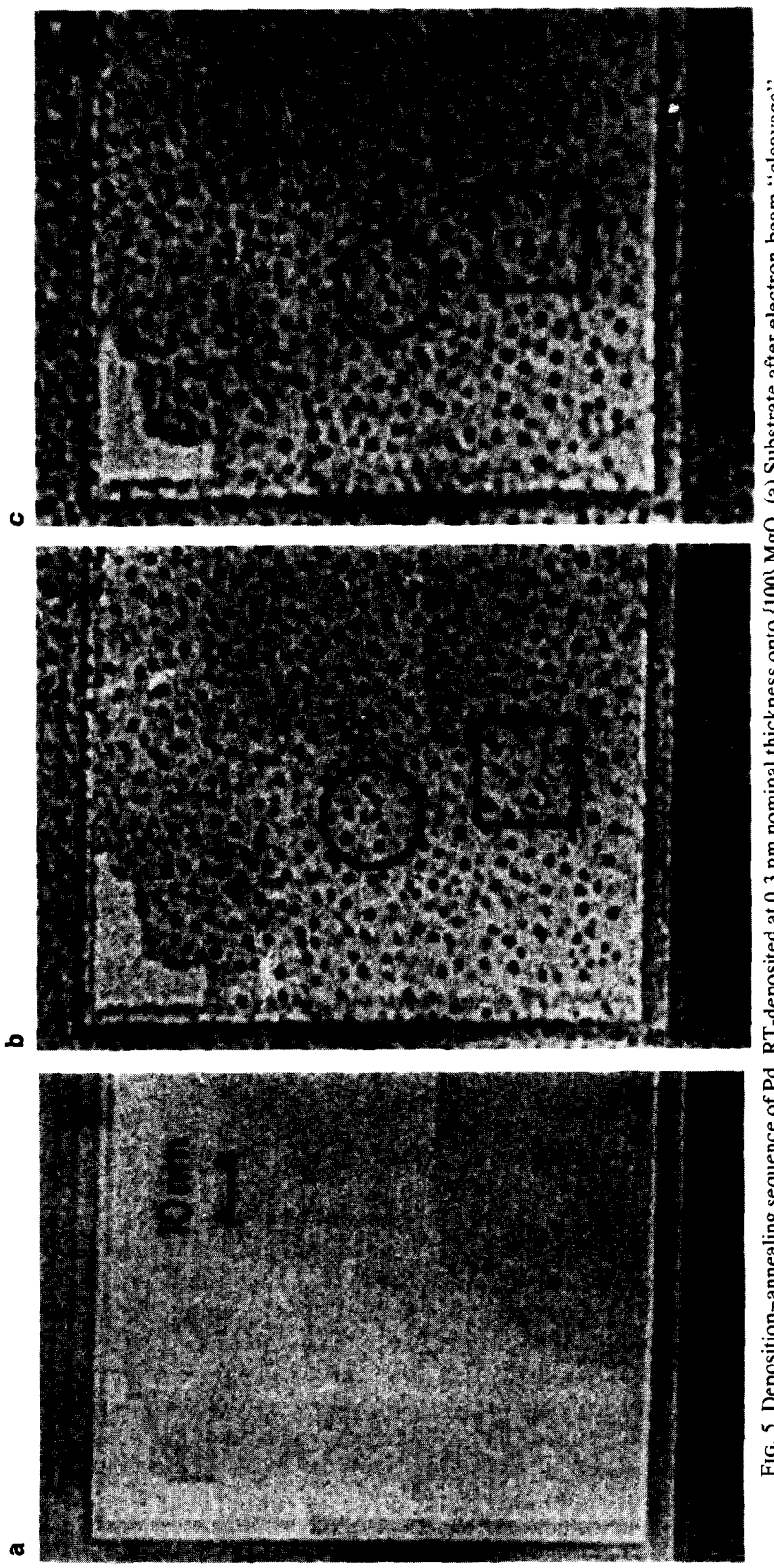

FIG. 5. Deposition–annealing sequence of Pd, RT-deposited at 0.3 nm nominal thickness onto {100} MgO. (a) Substrate after electron-beam "cleavage" before deposition; (b) shortly after deposition; (c) after deposition and 21 h in 1×10^{-8}-mbar background vacuum (circle indicates example of particle coalescence, square of mobility).

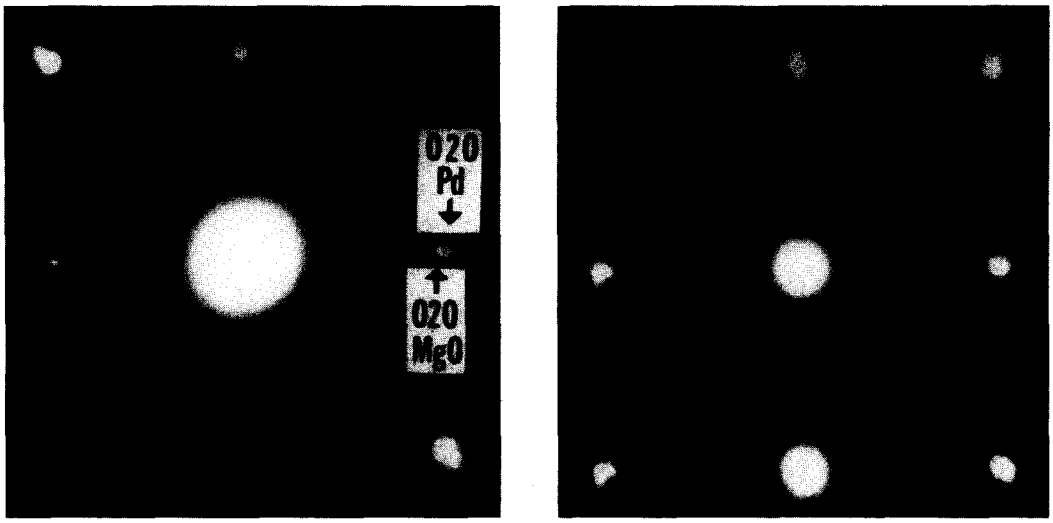

FIG. 6. Typical selected-area diffraction pattern of Pd/MgO {100} of 1.2 nm (left) and 1.8 nm (right) nominal thickness.

ygen at 2×10^{-6} mbar oxygen); significant spreading of some of the Pd particles occurred on the {111} substrate area (see circled area as an example), and almost complete spreading, leading essentially to disappearance of most of the Pd particles, was observed in the {100} MgO areas (top of Fig. 10).

Electron-Beam Induced Effects

Figure 11 demonstrates the typical influence of strong electron-beam irradiation of the sample (about 10 times larger dose than normally used for these studies). During the electron microscopy leading to Fig. 11c, a total beam exposure of 180 A s/cm^2 was logged. The irradiation was then intentionally prolonged by another 150 A s/cm^2 at a slightly increased current density, leading to Fig. 11d. A twofold effect is noticed. First, a build-up of material, similar in appearance to hydrocarbon contamination, has occurred, as can be seen along the edge of the MgO substrate area. However, particle mobility was not suppressed as would be expected from a typical hydrocarbon contamination "fixing" layer. (Considering the cleavage mechanism, which generates an area devoid of hydrocarbons regardless of the history of the sample, and the vacuum level maintained during these experiments, we can exclude hydrocarbon contamination in our experiments.) Second, strong phase contrast features appear along the left-hand side of the selected micrograph area, concomitant with a decrease of contrast and/or complete disappearance of the Pd particles. More careful examination of micrographs of this kind revealed that this effect is enhanced with increasing specimen thickness, as would be expected of radiation damage in the bulk of the MgO support.

We observed a significant enhancement of the radiation damage effect when the specimen had also been exposed to laboratory air at atmospheric pressure (inside the EM specimen stage for a few minutes). In this case, both particle spreading and generation of phase contrast features was already evident upon a beam exposure of only 30 A s/cm^2. The magnitude of this effect again increases with sample thickness.

A certain, not negligible effect of electron irradiation damage was noted also for plain MgO substrates without Pd deposit. However, the irradiation dosage until visible damage occurs is much higher (some 300 A

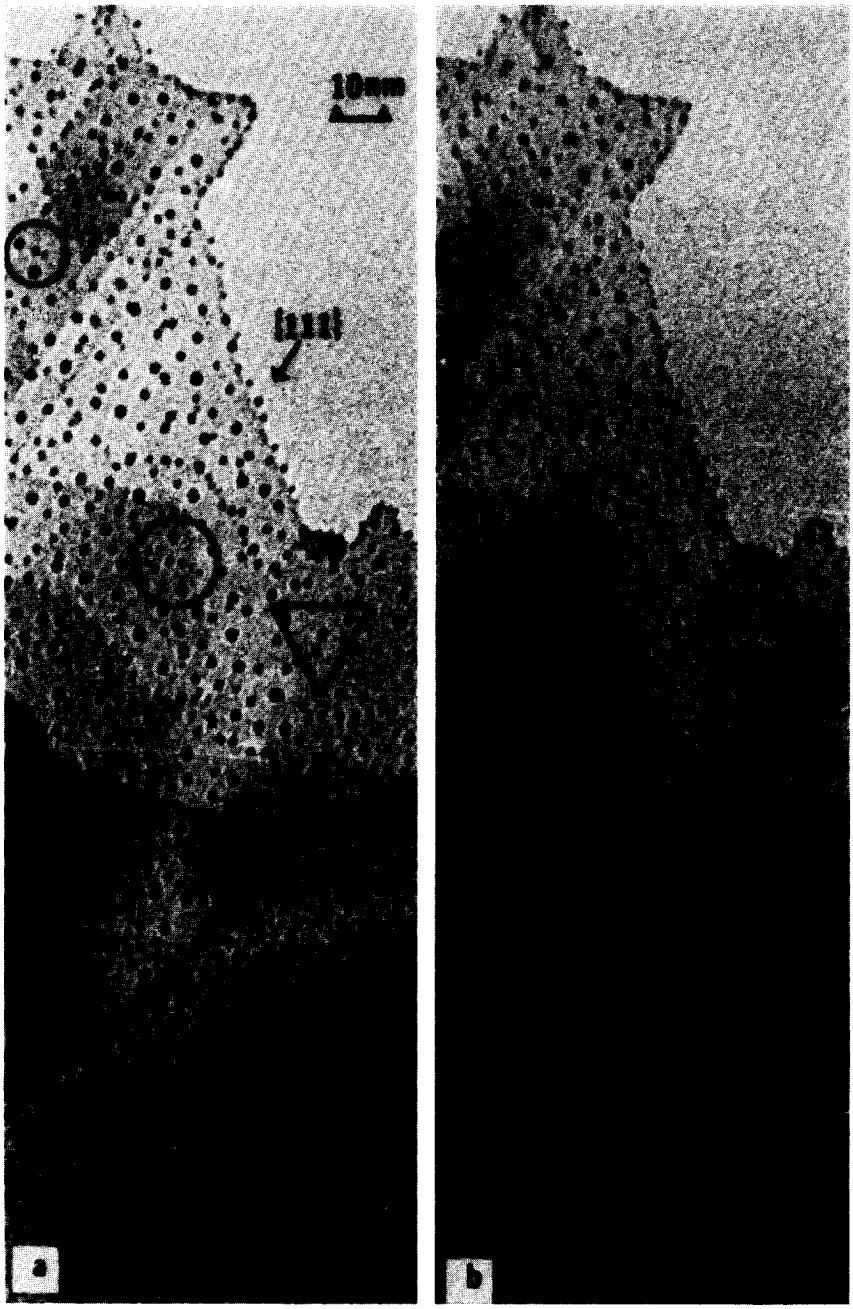

FIG. 7. Pd/MgO (0.3-nm nominal thickness) 7 min after deposition (a); and 2.5 min after exposure to oxygen for 3 min at 2×10^{-6} mbar (b). Circles indicate examples of coalescence, triangle points out shape change.

s/cm^2 for thick substrate areas), and no air exposure effect was observed in this case.

DISCUSSION

(1) *Epitaxy and Pseudomorphism*

The results indicate that palladium grows perfectly epitaxially on MgO at temperatures as low as RT. In contrast, epitaxy on sapphire surfaces under otherwise identical *in situ* TEM conditions requires a substrate temperature of 500°C (*9*). A comparatively low epitaxial temperature (T_e) for Pd was found by various other investigators: Doering *et al.* (*10*) found a slight texture for Pd/mica at 200°C. Christman and Ertl (*11*) report an optimum temperature for Pd/NaCl of 200°C, with 100 or 300°C yielding strong fiber textures. Murr and collaborators (*12*) reached essentially the same conclusion. Kato (*13*), working under 10^{-5}-mbar vacuum conditions, found an increase of T_e for Pd/KCl and Pd/KBr to Pd/KI from 80 to 280°C and suggests a correlation between T_e and the ionic radius of the anions in the substrate. Gillet and Renou (*14*) found good epitaxy for Pd/MoS_2 over a wide range of substrate temperatures (T_s). Takayanagi *et al.* actually performed Pd/MgO studies under conditions similar to ours, but only at elevated substrate temperatures between 200 and 500°C, and in this regime they found perfect Pd/MgO epitaxy (*15*). Similarly, Palmberg and Rhodin (*16*) obtained {100} epitaxy for Pd/MgO (bulk, uhv-cleaved) for $T_s > 350$°C.

The low epitaxial temperature for Pd/MgO compares with a much higher epitaxial temperature for Pd/sapphire under otherwise very comparable conditions (*9*). This is another indication that the geometric registry between overgrowth and substrate (8% for bulk Pd/MgO, less for Pd/sapphire) is often not the deciding factor in the determination of epitaxy (*17*). Surface free energy considerations (*17*) and electronic interactions between overgrowth and support (*18*) are usually more important factors for determining the mode of overgrowth (layer vs three-dimensional deposits) and epitaxy.

One of the more surprising results of this study is that the lattice parameter of Pd on {100} MgO was found expanded by some 3% when compared to the bulk parameter, and the diffraction spots were unusually broad (Fig. 6). The expansion was highest for the smallest particles. Some broadness of the Pd diffraction spots is due to the small size of the Pd islands (diffraction broadening). However, our results cannot fully be explained on this basis. Using the mean particle sizes computed with Eq. (2), Scherrer broadening (*19*) would cause the Gaussian spot size distributions shown in part A of Fig. 12 for the nominal deposit thicknesses 0.3–1.8 nm (the integrated intensity was set proportional to the deposit thickness). Averages of many diffraction patterns such as those shown in Fig. 6 give, on the other hand, the diffraction intensity distributions shown in part B of Fig. 12. It is evident that (i) the actual spot sizes are much broader than would be expected if only standard line broadening would be present, and (ii) that the tendency of the broadening direction is toward a decrease of the Pd/MgO lattice misfit, which is about 8% for bulk Pd/MgO; i.e., the tendency is for the Pd lattice parameter to increase with respect to the bulk lattice parameter.

A number of researchers have investigated the lattice parameters of small particles, and a spectrum from some lattice contraction (*15, 20–25*) to substantial expansion (*25–29*) has been reported for various metal/substrate systems and experimental conditions. Work is underway to perform computer simulated diffraction at very small particles. First results of this work indicate that an apparent lattice expansion can be expected in the diffraction pattern of very small particles as a genuine diffraction effect and not as intrinsic particle property. A report of these results is in preparation (*30*).

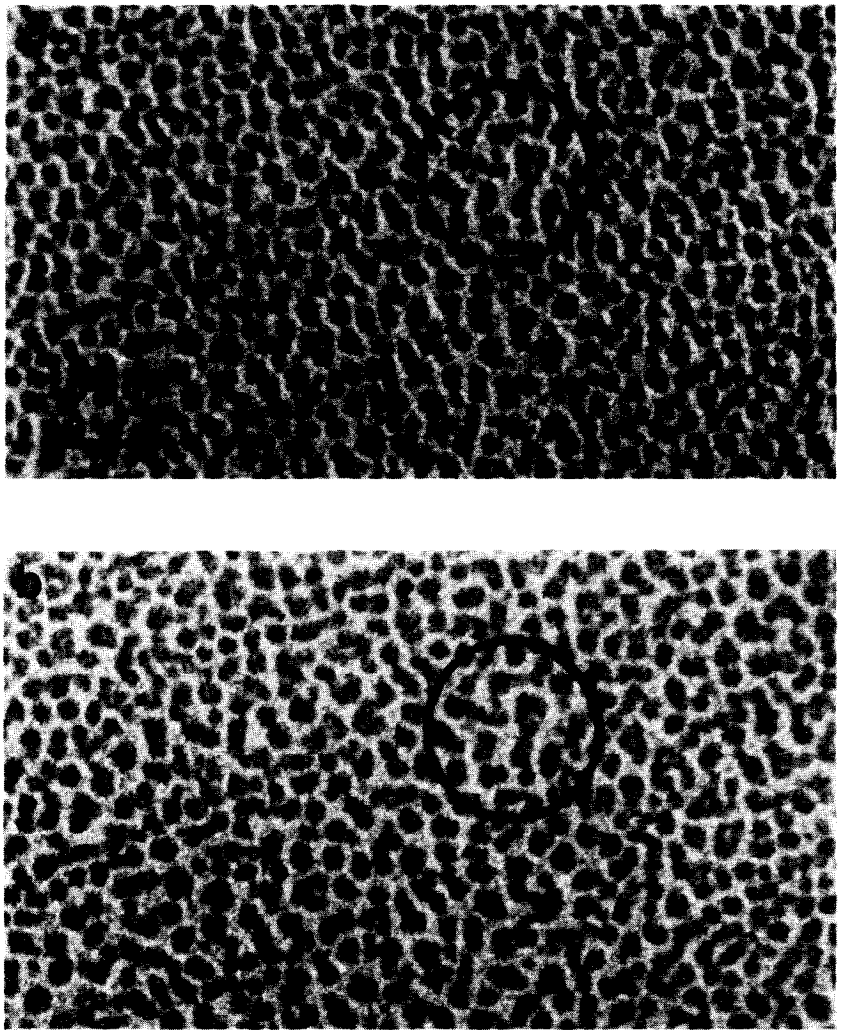

FIG. 8. Pd/MgO {100} (1.8 nm nominal thickness) shortly after deposition (a); after 10 min exposure to laboratory air (b); after 30 additional minutes of exposure to air (transfer to other microscope, (c)); and after 120-hr exposure to laboratory air (d). Circle depicts randomly selected area for easier comparison.

(2) *Annealing, Gas Exposures, and Electron-Beam Enhancement*

The results indicate that annealing *in vacuo* at room temperature, exposure to gases, and exposure to the electron beam all influence the deposit. Due to the nature of *in situ* TEM experiments that are performed sequentially and rely on the electron beam for recording purposes, one cannot positively study the effect of any one of these factors independent of the others. The design of the experiments allowed, however, a partial assessment of the influence of these parameters on the Pd particles on MgO. The following trends can be extracted from our results:

(i) The effect of annealing at RT under 1 $\times 10^{-8}$-mbar vacuum conditions is some coalescence by cluster mobility. Similar to our findings in earlier experiments, where we examined *in situ* the annealing behavior

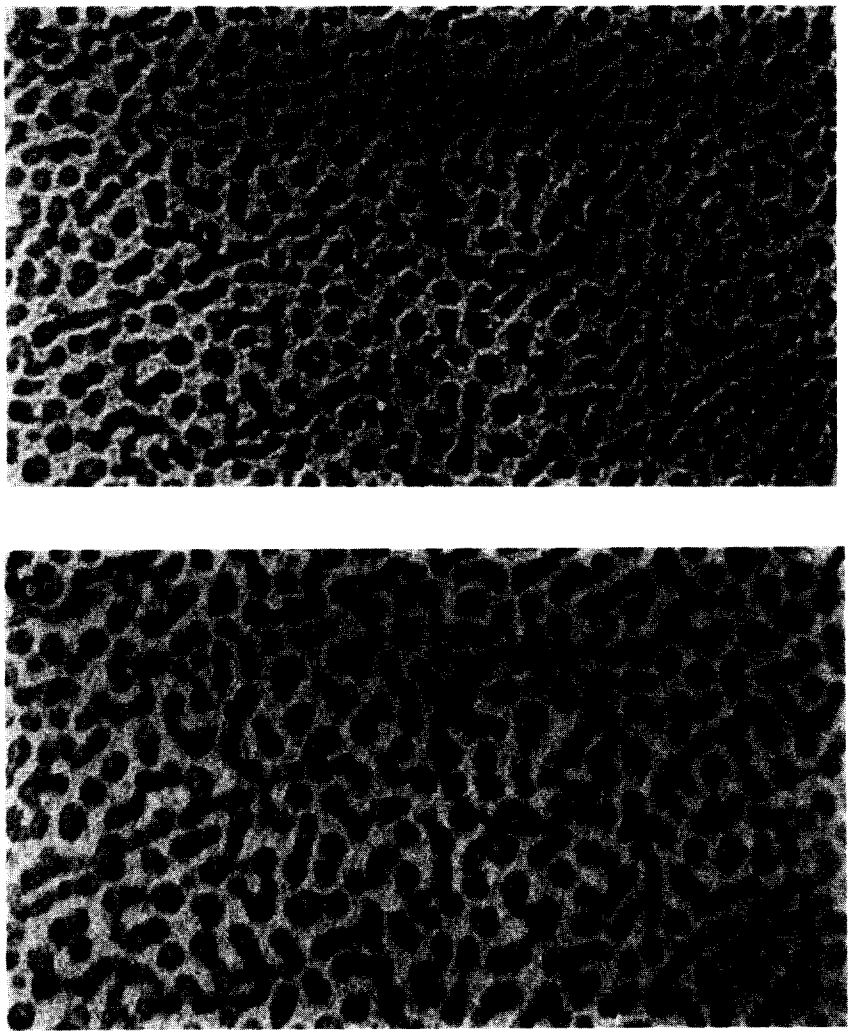

FIG. 8—*Continued.*

of silver on graphite (*31*) and gold on MgO (*4, 32*), we conclude also for the present experiments that Ostwald ripening can be excluded as a major factor.

(ii) The particles coalescing during RT vacuum annealing do often not sinter into a new, hemispherically shaped single crystal particle, but they rather form "rafts" of particles, leaving the area coverage of the substrate with particles essentially unchanged. This finding indicates that in the case of Pd/MgO the second of the two steps (*31*) comprising full coalescence, i.e., the sintering to a homogeneous new particle, does usually not occur. One possible explanation for this observation might be a strong interaction of the palladium with the substrate, thus making diffusion of Pd atoms away from a position near the substrate surface for incorporation into a newly forming, larger particle less likely.

(iii) The high vacuum, RT annealing effect is relatively strongest for the smallest particle sizes, i.e., for thin deposits. This observation is in general agreement with most other small-particle mobility work reported and is usually explained by proportionality of the activation energy for cluster

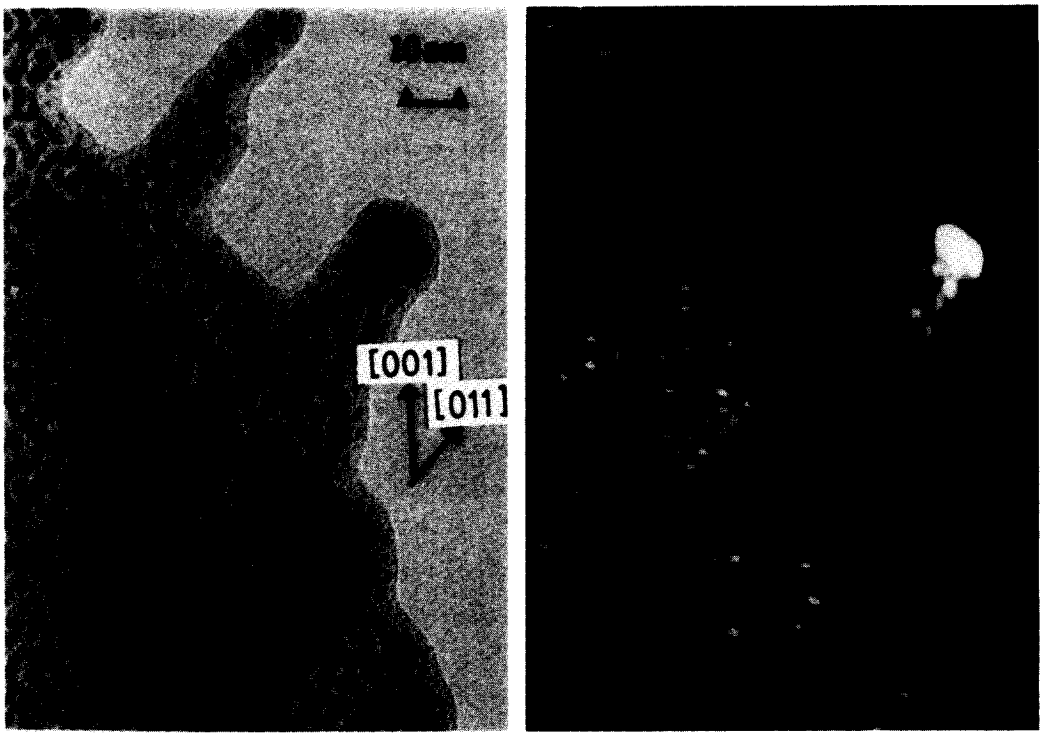

FIG. 9. Long-term air-exposed Pd/MgO {100}. Left: BF-image; right: Pd 200 SZDF image.

mobility to the cluster/substrate contact area.

(iv) The annealing effect is greatly enhanced upon sample exposure to laboratory air or to a low-pressure oxygen environment (see Fig. 8 for a heavy Pd deposit on MgO for the case of air exposure, and Fig. 10 for an oxygen exposure). It is assumed that the oxygen reduces the activation energy for particle mobility. Once exposed to oxygen or laboratory air, the enhanced annealing effect seems to continue for long periods of time (tens of hours, Figs. 8 and 10), whereas it seems to subside comparatively quickly without oxygen or air (Figs. 5 and 11).

(v) Some effect of minimum-intensity electron irradiation upon the observed particle mobility events cannot be categorically excluded at the present time. The observation that phase contrast-like (radiation damage) features appear appreciably sooner when the Pd/MgO deposit has been exposed to air or low-pressure oxygen, compared to electron irradiation of unexposed samples, indicates at least for stronger irradiation dosages a beam/deposit/substrate interaction. It is conceivable that at 1 or 2 orders of magnitude lower radiation dosages (the conditions prevailing during most of our TEM observations) some electron-beam influence is present even though it is not directly apparent in the TEM image.

More extensive gas exposure studies are the subject of a separate report, in which an attempt is made to correlate particle mobilities and flattening effects with the influence of various gases, in particular oxygen, on the Pd particle/MgO substrate interaction (*33*).

CONCLUSIONS

Palladium particles were grown inside a custom TEM specimen chamber onto clean MgO {100} and {111} surfaces prepared by electron-beam flash heating. TEM exami-

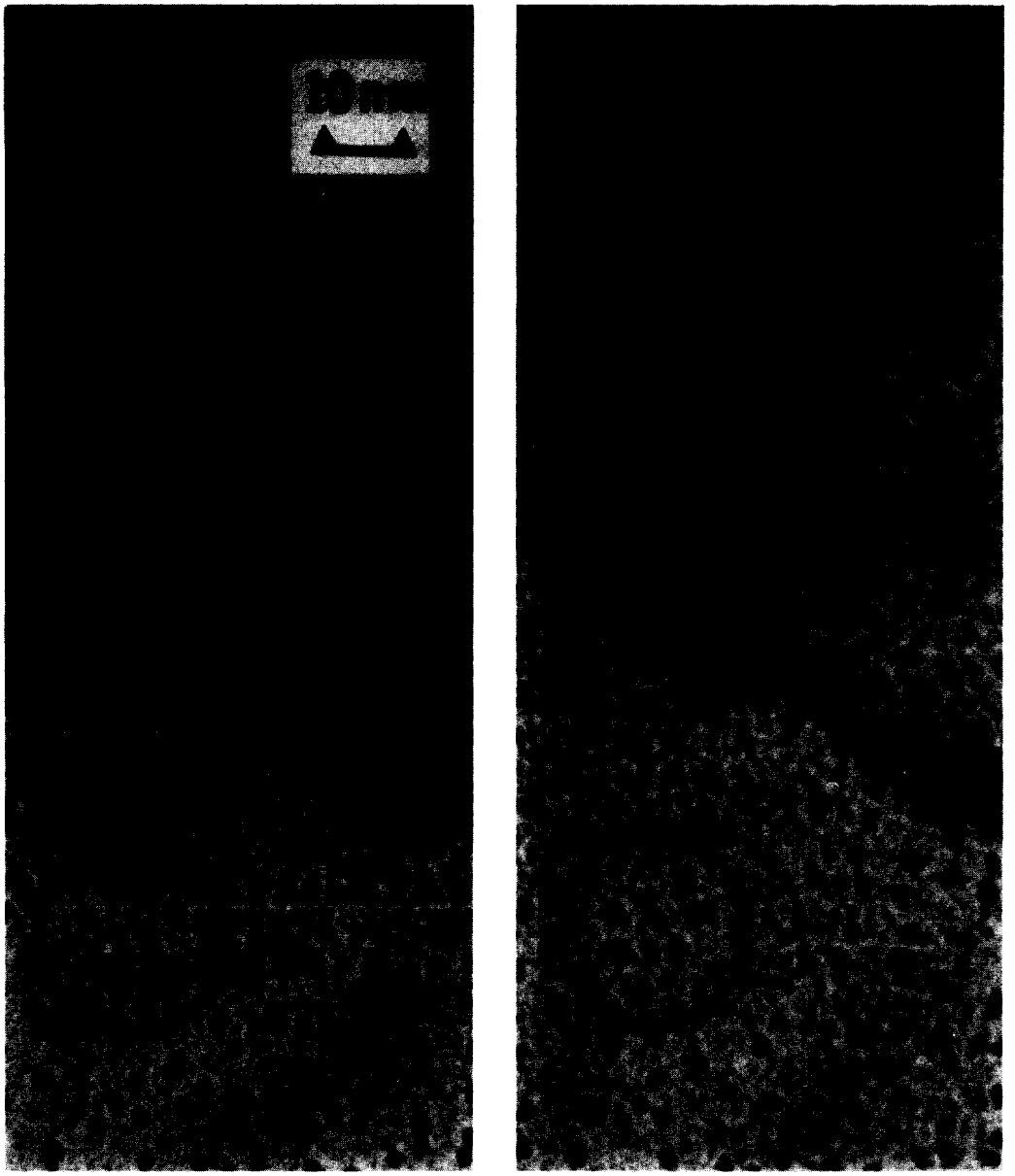

FIG. 10. Pd/MgO ({111} area in lower half, {100} area in upper half; 0.3 nm nominal deposit thickness); left: 40 min after 3-min oxygen exposure at 2×10^{-6} mbar, right: 100 h later. Note particle flattening.

nation of deposits of 0.3–1.8 nm nominal thickness (with particle sizes from 1–5 nm) yielded results that suggest a strong interaction between the substrate and the metal deposit. These results include:

(i) Perfect epitaxy already for room-temperature deposits;

(ii) Apparent expansion of the Pd lattice by some 2–4%, the largest amounts of expansion being registered for the smallest particles;

(iii) A spreading of the Pd islands on the MgO substrate upon long-term (tens of hours) high-vacuum annealing at RT after

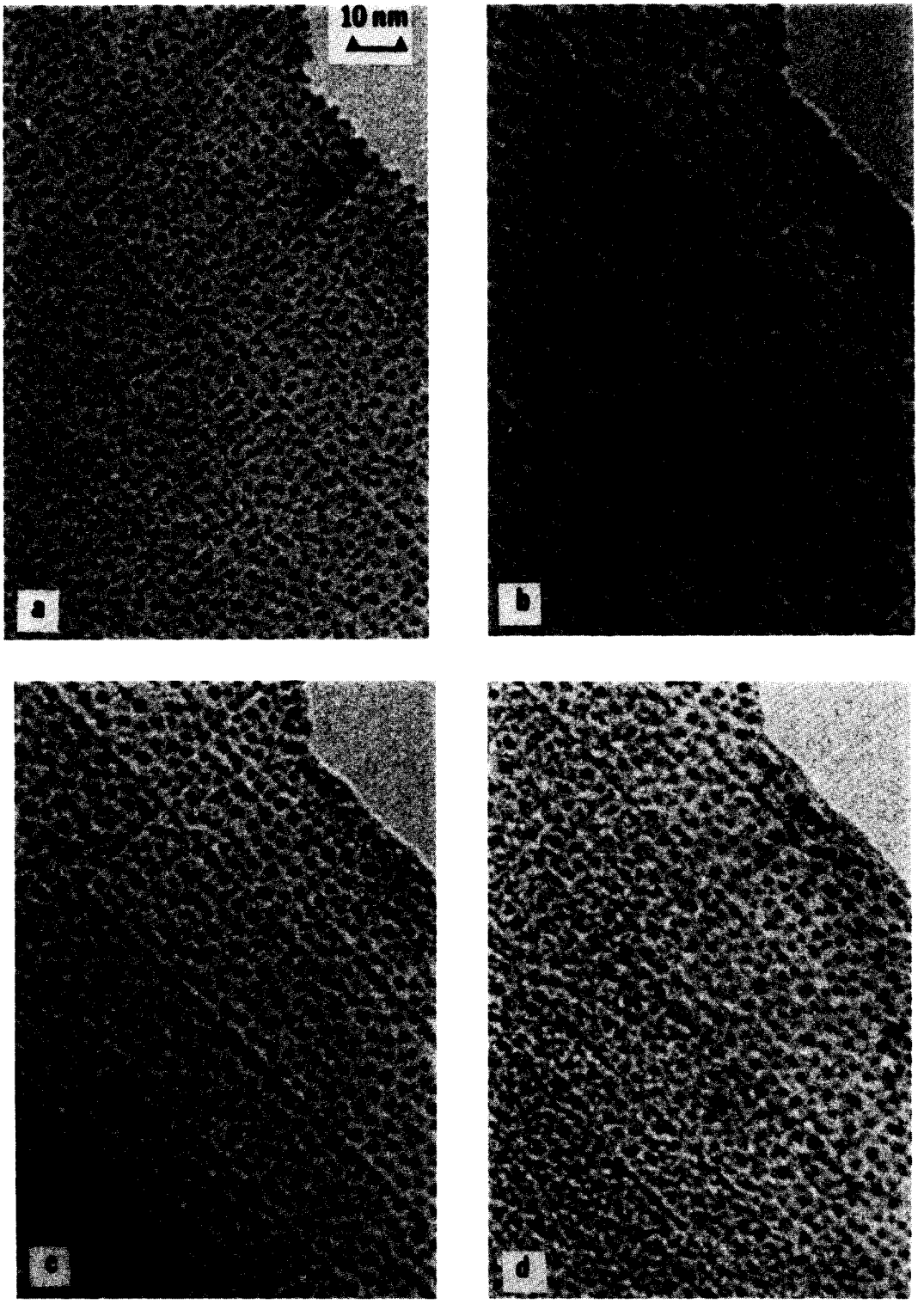

FIG. 11. Effect of intense electron-beam exposure of Pd/MgO {100} (0.6 nm nominal thickness); (a) immediately after end of deposition; (b) 200 min later; (c) and (d) 15 hr later; (d) has obtained 150 A s/cm^2 additional electron irradiation, causing radiation damage-induced particle flattening.

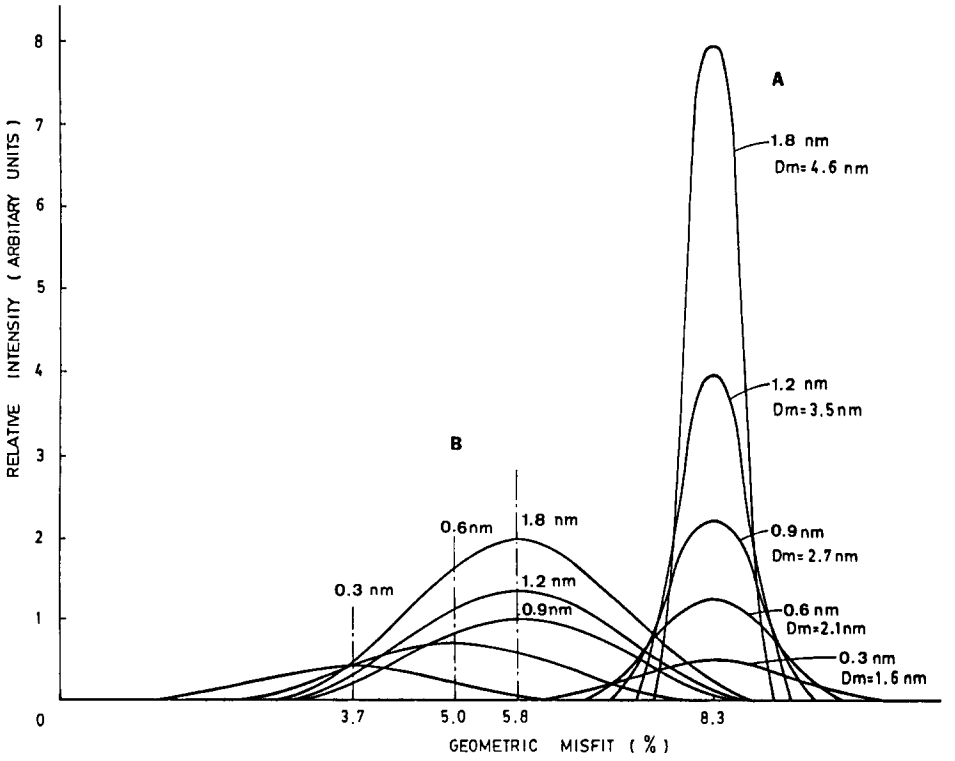

FIG. 12. Intensity distributions across Pd diffraction spots for various mean particles sizes, computed with Eq. (4) (A); and as measured for Pd/MgO (B).

short exposure to laboratory air or oxygen;

(iv) Strong coalescence with subsequent minimization of the surface area of the coalesced particles during long-term (tens of hours) RT exposure to laboratory air, and

(v) Some effect of strong electron-beam irradiation, which leads to the conclusion that a finite effect of the electron beam upon the mobility results cannot be excluded a priori; future studies will have to address this difficult problem.

The experiments clearly indicate that one would be well advised to exercise caution in the interpretation of *ex situ* TEM results obtained from particulate metal deposits on refractory oxide supports that have been exposed to laboratory air during the TEM specimen preparation process. Substantial changes in particle habit and crystal structure, as well as size, area coverage of the substrate, and number density may occur. Changes may be experienced due to exposure of only a few tens of Langmuirs of gases such as oxygen or air, or even due to mere RT-annealing in 1×10^{-8}-mbar background vacuum. These findings underline the importance of *in situ* TEM observations when characterizing supported particle systems of importance to catalysis. Further studies of different metal/support material combinations are in progress.

ACKNOWLEDGMENTS

This work was supported by NASA Grant NCC 2-171. Financial support by Waseda University, Tokyo, Japan (for T.O.) and by the Universidad Nacional Autónoma de México (for M.A.) is also greatly acknowledged.

REFERENCES

1. Poppa, H., and Heinemann, K., *Optik* **56,** 183 (1980).
2. Poppa, H., *Ultramicroscopy,* in press.
3. Honjo, G., Shinozaki, S., and Sato, H., *Appl. Phys. Lett.* **9,** 23 (1966).

4. Metois, J. J., Heinemann, K., and Poppa, H., *Thin Solid Films* **41,** 197 (1977).
5. Heinemann, K., and Osaka, T., *J. Cryst. Growth* **59,** 485 (1982).
6. Heinemann, K., Anton, R., and Poppa, H., *Proc. 39th Annu. Meet. Electron Microsc. Soc. Am.* 158 (1982).
7. Heinemann, K., Kim, H. K., and Poppa, H., *J. Vac. Sci. Technol.* **16,** 622 (1979).
8. Heinemann, K., and Poppa, H., *Appl. Phys. Lett.* **20,** 122 (1972).
9. Heinemann, K., Osaka, T., and Poppa, H., to be published.
10. Doering, D. L., Poppa, H., and Dickinson, J. T., *J. Catal.* **73,** 104 (1982).
11. Christmann, K., and Ertl, G., *Thin Solid Films* **28,** 3 (1975).
12. Murr, L. E., *Thin Solid Films* **7,** 101 (1971).
13. Kato, T., *Jpn. J. Appl. Phys.* **7,** 1162 (1968).
14. Gillet, M., and Renou, A., *Thin Solid Films* **52,** 23 (1978).
15. Takayanagi, K., Yagi, K., and Honjo, G., *Thin Solid Films* **48,** 137 (1978).
16. Palmberg, P. W., and Rhodin, T. N., *J. Chem. Phys.* **49,** 134 (1968).
17. Bauer, E., and Poppa, H., *Thin Solid Films* **12,** 167 (1972).
18. Ryndin, Yu, Hicks, R. F., and Bell, A. T., *J. Catal.* **70,** 287 (1981).
19. Scherrer, P., *Goettinger Nachrichten* **2,** 98 (1918).
20. Poppa, H., Heinemann, K., and Elliot, A. G., *J. Vac. Sci. Technol.* **8,** 471 (1971).
21. Gallezot, P., *Surf. Sci.* **106,** 459 (1981).
22. Mays, C. W., Vermaak, J. S., and Kuhlmann-Wilsdorf, D., *Surf. Sci.* **12,** 134 (1968).
23. Boswell, F. W. C., *Proc. Phys. Soc. London Sect. A* **64,** 465 (1951).
24. Woltersdorf, J., Nepijko, A. S., and Pippel, E., *Surf. Sci.* **106,** 64 (1981).
25. Yokozeki, A., *J. Chem. Phys.* **68,** 3766 (1978).
26. Burton, J. J., and Jura, G., *J. Phys. Chem.* **71,** 1937 (1967).
27. Tick, P. A., and Witt, A. F., *Surf. Sci.* **26,** 165 (1971).
28. Anton, R., and Poppa, H., "Proceedings, 10th International Congress on Electron Microscopy, Hamburg," Vol. 2, pp. 509 and 511. 1982.
29. Turkevich, J., Ban, L. L., and Wall, J. H., *in* "Perspectives in Catalysis in Commemoration of Jons Jacob Berzelius" (R. Larsson, Ed.), p. 59. University of Lund, Sweden, Oct. 1979.
30. Avalos-Borja, M., Poppa, H., and Heinemann, K., to be published.
31. Heinemann, K., and Poppa, H., *Thin Solid Films* **33,** 237 (1976).
32. Metois, J. J., Heinemann, K., and Poppa, H., *Philos. Mag.* **35,** 1413 (1977).
33. Heinemann, K., Osaka, T., and Poppa, H., *Ultramicroscopy,* in press.